

Frequency Response Data Based LPV Controller Synthesis Applied to a Control Moment Gyroscope

Tom Bloemers, Roland Tóth and Tom Oomen

Abstract—Control of systems with operating condition-dependent dynamics, including control moment gyroscopes, often requires operating condition-dependent controllers to achieve high control performance. The aim of this paper is to develop a frequency response data-driven linear parameter-varying control design approach for single-input single-output systems, which allows improved performance for a control moment gyroscope. A stability theory using closed-loop frequency response function data is developed, which is subsequently used in a synthesis procedure that guarantees local stability and performance. Experimental results on a control moment gyroscope demonstrate the performance improvements.

I. INTRODUCTION

Control of systems with operating condition-dependent dynamics, including control moment gyroscopes (CMGs), often requires operating condition-dependent controllers to achieve high control performance. CMGs are attitude control devices used, e.g., to control the attitude of spacecraft [1]. A CMG, see Figure 1a, consists of a rotating disk, which, when spinning, generates an angular momentum. The disk is mounted in a gimbal assembly which can rotate around multiple axes. Changing the direction of the angular momentum vector, through actuation of the gimbals, generates a gyroscopic torque [2]. This torque can be used to, e.g., change the attitude of a spacecraft. The associated dynamics are nonlinear and characterized by coupled behavior and challenging rotational dynamics that change based on the operating conditions of the system. Locally, these behaviors manifest in terms of operating condition-dependent resonant dynamics, also commonly encountered in mechatronic systems [3]. Flexible phenomena introduce severe practical limitations on the achievable performance, which become even more severe in case of operating condition-dependent dynamics. Achieving stability and high performance for these systems requires operating-condition dependent controllers [4], [5].

The paradigm of linear parameter-varying (LPV) systems has been established to provide a systematic framework to efficiently handle operating condition-dependent nonlinear dynamics. LPV systems are characterized by a linear input-output (IO) map, whose dynamics depend on an exogenous time-varying signal. This scheduling variable p can be used to capture the nonlinear or operating condition-dependent

dynamics of a system. Typically, a priori information on the scheduling variable is known, such as the range of variation. LPV systems are supported by a well-developed model-based control and identification framework, with many successful applications, see [3], [6]. Model-based control techniques require an accurate parameter-dependent parametric model of the system suitable for LPV control design. In fact, obtaining such a high accuracy model is a challenging task, even for linear time-invariant (LTI) systems [7].

Frequency response function (FRF) measurements enable systematic design of controllers directly from measurement data and are commonly employed in the industry [7]. A frequency response function estimate provides an accurate nonparametric description of the system that is relatively fast and inexpensive to obtain [8]. Also the nonparametric identification of local FRF measurements for LPV systems has been investigated in [9], assuming that the underlying behavior is a smooth function of the scheduling variable. For the CMG, FRFs of the local dynamics can be accurately captured at a set of operating points. FRFs enable the use of classical techniques such as loop-shaping, alongside graphical tools including the Bode diagram or Nyquist plot, to design controllers [10]. These controllers often have a proportional-integral-derivative (PID) structure in addition to higher-order filters to compensate parasitic dynamics. These methods have in common that the design procedure can be difficult as they are based on design rules, insight and experience.

Data-driven control design based on FRF measurements provides systematic approaches to design and synthesize LTI controllers. From a modeling perspective, data-driven control synthesis provides an alternative to control-oriented identification [11]. At first, the development of these methods have been along the lines of the classical control theory to tune PID controllers [12]. Later, these methods have been tailored towards more general control structures that focus on \mathcal{H}_∞ -performance [13]. The incorporation of model uncertainties into the control design enables the synthesis of stabilizing controllers that achieve sufficient robustness to account for the variations in the plant [14], [15]. Robust control methods are attractive to accommodate the operating condition-dependent resonant behaviors encountered in CMGs. A major drawback is a tradeoff between robustness and performance.

Including operating condition-dependent behavior in the data-driven control design framework is promising to overcome the tradeoff between robustness and performance. In [16], a time-domain approach is employed to identify an LPV controller such that the closed-loop mimics an ideal behavior. In [17]–[19], frequency-domain control synthesis approaches are investigated. Common drawbacks are their limitations to

T. Bloemers (corresponding author) and R. Tóth are with the Control Systems Group, Department of Electrical Engineering, Eindhoven University of Technology. T. Oomen is with Control Systems Technology, Department of Mechanical Engineering, Eindhoven University of Technology, email: {t.a.h.bloemers, r.toth, t.a.e.oomen}@tue.nl. R. Tóth is also with the Systems and Control Laboratory, Institute for Computer Science and Control, Kende u. 13-17, H-1111 Budapest, Hungary.

This work has received funding from the European Research Council (ERC) under the European Union's Horizon 2020 research and innovation programme (grant agreement nr. 714663).

stable systems only, conservative stability and performance constraints and the controller parameterization only allows for shaping of the zeros and not the poles.

Although frequency-domain data-driven controller synthesis enables powerful and systematic design approaches in the LTI framework, methods within the LPV framework are limited and conservative. The aim in this paper is to develop a data-driven LPV control design method that allows both for stable and unstable systems, applicable to an experimental CMG setup. Key steps are (i) a global LPV controller parameterization, which allows tuning of both the zeros and poles based on local information, and (ii) developing necessary and sufficient stability and performance analysis conditions.

The main contributions of this paper are

- C1) A procedure to synthesize LPV controllers for (possibly) unstable single-input single-output (SISO) plants from frequency-domain measurement data, with local internal stability and \mathcal{H}_∞ -performance guarantees.
- C2) Highlighting the advantages of using an LPV controller through application to an experimental CMG setup.

This is achieved by the following sub-contributions.

- C3) Developing of a local LPV frequency-domain stability analysis condition.
- C4) Development of a local LPV frequency-domain \mathcal{H}_∞ -performance analysis condition.

Contributions C3) and C4) are generalizations to the results presented in [15], [20]. Specifically, when both the plant and controller are LTI the results in [15] are recovered, and the results in [20] are recovered as a special case for stable systems. Other important differences in this paper are new insights and proofs of these sub-contributions, which establish links to the robust control theory and the Bézout identity. A global LPV controller parameterization in combination with C3) and C4) constitutes to C1). Application of the developed procedures on an experimental CMG constitutes to C2).

Notation: Let \mathbb{R} denote the set of real numbers and \mathbb{C} the set of complex numbers. Let \mathbb{C}_0 denote the imaginary axis and \mathbb{C}_+ the open right half-plane. The real part of a complex number $z \in \mathbb{C}$ is denoted by $\Re\{z\}$. The set of proper, stable and real-rational transfer functions is denoted by \mathcal{RH}_∞ .

Remark. *Although the theory in this paper is presented in continuous-time, a discrete-time equivalent is conceptually straightforward. Simply replace the variables s with z , $i\omega$ with $e^{i\omega}$ and evaluate the frequencies along the unit circle instead of the imaginary axis, i.e., for the set $\Omega := \{\omega \mid 0 \leq \omega < 2\pi\}$.*

II. PROBLEM FORMULATION

A. Control Moment Gyroscope

Figure 1a depicts the considered 3 degree of freedom (DOF) control moment gyroscope. It is comprised of a disk, D , which is mounted in a gimbal assembly consisting of three gimbals C , B and A , corresponding to the schematic overview in Figure 1b. The disk D rotates with velocity \dot{q}_1 , generating an angular momentum proportional to \dot{q}_1 . Angle q_2 of gimbal C is controlled through input torque τ_2 . Gimbal B is assumed to be fixed in place such that $q_3 \equiv 0$, as depicted in Figure 1b. Angle q_4 of gimbal A is controlled through a gyroscopic

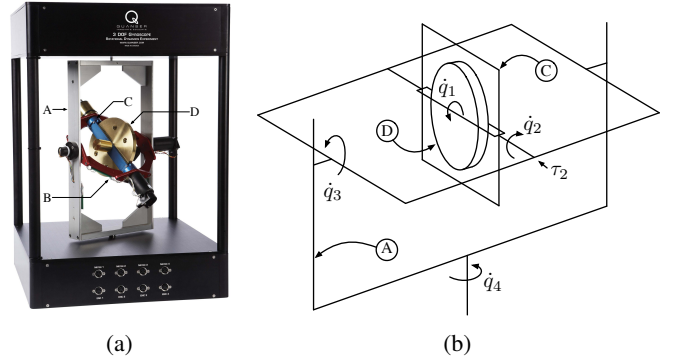


Fig. 1: Laboratory scale control moment gyroscope by Quanser (a); and schematic overview of the 3-DOF gyroscope (b).

torque, generated by changing angle q_2 . As the disk tilts, a change in angular momentum causes gyroscopic torque, which is used to position gimbal A .

The equations of motions are of the form

$$\mathcal{M}(q(t))\ddot{q}(t) + \mathcal{C}(q(t), \dot{q}(t))\dot{q}(t) = \tau_2(t), \quad (1)$$

where $q^\top = [q_1 \ q_2 \ q_4]$ are the angular positions, τ_2 is the input torque, \mathcal{M} and \mathcal{C} are the inertia and Coriolis matrices.

In the used configuration of the CMG, the goal is to control the position of gimbal A by actuating gimbal C through input torque τ_2 . The driving factor in this setting is the velocity of the disk D , which directly relates to the amount of gyroscopic torque that can be exerted on gimbal A . In [4], it is shown that local linear approximations describe the nonlinear dynamics accurately. The aggregated collection of these local approximations is described by the following representation

$$\dot{x}(t) = A(\dot{q}_1(t))x(t) + Bu(t), \quad (2a)$$

$$y(t) = q_4(t), \quad (2b)$$

where $x^\top = [q_4 \ \dot{q}_2 \ \dot{q}_4]$ is the state, $u = \tau_2$ the input and $y = q_4$ the output. The A matrix depends on the velocity of the disk, which can range anywhere in $\dot{q}_1 \in [30, 50]$ rad/s.

The local description of the behavior is in line with the availability of measurement data and the considered control synthesis techniques in the sequel. Furthermore, the dependence of the system on the disk velocity makes the LPV framework a suitable choice for modeling and control.

B. LPV systems

Consider a single-input single-output, continuous-time (CT) LPV system. The LPV state-space representation

$$G_p : \begin{cases} \dot{x}(t) &= A(p(t))x(t) + B(p(t))u(t), \\ y(t) &= C(p(t))x(t) + D(p(t))u(t), \end{cases} \quad (3)$$

is adopted to represent the system, see also [21]. Here, $x : \mathbb{R} \rightarrow \mathbb{X} \subseteq \mathbb{R}^{n_x}$ denotes the state variable, $u : \mathbb{R} \rightarrow \mathbb{U} \subseteq \mathbb{R}$ is the input signal, $y : \mathbb{R} \rightarrow \mathbb{Y} \subseteq \mathbb{R}$ is the output signal and $p : \mathbb{R} \rightarrow \mathbb{P} \subseteq \mathbb{R}^{n_p}$ the scheduling variable.

With a slight abuse of notation introduce

$$G_p = \left(\begin{array}{c|c} A(p) & B(p) \\ \hline C(p) & D(p) \end{array} \right) \quad (4)$$

representing the LPV system with state-space form (3). If $D^{-1}(p)$ is well-defined for all $p \in \mathbb{P}$, then the LPV system

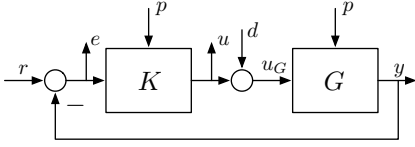


Fig. 2: Typical 1 DOF feedback interconnection, including 4-block shaping problems, depending on the scheduling signal.

G_p has an inverse operator

$$G_p^{-1} = \left(\begin{array}{c|c} A(p) + B(p)D^{-1}(p)C(p) & B(p)D^{-1}(p) \\ \hline D^{-1}(p)C(p) & D^{-1}(p) \end{array} \right), \quad (5)$$

such that $G_p G_p^{-1} = G_p^{-1} G_p = 1$ for all $p \in \mathbb{P}$.

If the scheduling signal $p(t) \equiv p$ is constant, the scheduling-dependent matrices in (4) become time-invariant, i.e.,

$$G_p = \left(\begin{array}{c|c} A(p) & B(p) \\ \hline C(p) & D(p) \end{array} \right) \quad (6)$$

represents an LTI system for constant scheduling. For a given $p \in \mathbb{P}$, (6) describes the local behavior of (3). Hence, (6) is referred to as the frozen behavior of (3). Taking the Laplace transform of (6) with zero initial conditions results in

$$\hat{y}(s) = (C(p)(sI - A(p))^{-1}B(p) + D(p)) \hat{u}(s), \quad (7)$$

where $G_p(s) = C(p)(sI - A(p))^{-1}B(p) + D(p)$ and s is the Laplace variable. The frozen behavior (6) also has a corresponding Fourier transform

$$Y(i\omega) = G_p(i\omega)U(i\omega), \quad (8)$$

where i is the complex unit, $\omega \in \mathbb{R}$ is the frequency and $G_p(i\omega)$ represents the frozen Frequency Response Function (fFRF) of (3) for every constant $p(t) \equiv p \in \mathbb{P}$ [22].

C. Problem statement

The problem addressed in this paper is to design an LPV controller directly from fFRF measurement data obtained from the considered CMG. We denote the data $\mathcal{D}_{N,p,\tau} = \{G_p(i\omega_k), p_\tau\}_{k=1}^N$, obtained at the set of operating points $\mathcal{P} = \{p_\tau\}_{\tau=1}^{N_{loc}} \subset \mathbb{P}$. We assume the frequencies are sufficiently dense such that it suffices to check a finite number of discrete points to draw conclusions on the underlying continuous curve. Consider the feedback interconnection in Figure 2. The objective is to design a controller K_p such that the following requirements are satisfied.

R1) The closed-loop system in Figure 2 is internally stable in the local sense for all $p(t) \equiv p \in \mathcal{P}$.

R2) The performance channels of the closed-loop system are bounded in the local \mathcal{H}_∞ -norm sense for all $p \in \mathcal{P}$.

In the next section, a rational controller parameterization is introduced that allows for a specific formulation of internal stability. This forms the basis to develop analysis conditions for internal stability and \mathcal{H}_∞ -performance. The theory is first formulated for $p \in \mathbb{P}$ for the sake of generality. This also ensures R1) and R2) for $p \in \mathcal{P}$.

III. STABILITY AND PERFORMANCE ANALYSIS

In this section, we develop local LPV stability and performance analysis conditions. These results form the basis for a data-driven synthesis procedure. First, a continuous frequency spectrum $\Omega = \{\mathbb{R} \cup \{\infty\}\}$ is considered, which will be

restricted later to a finite frequency grid $\Omega_N = \{\omega_k\}_{k=1}^N$ corresponding to $\mathcal{D}_{N,p,\tau}$.

A. Stability

The selection of input-output (IO) pairs in Figure 2 corresponds to the problem of internal stability [23, Chapter 3]. For a fixed $p \in \mathbb{P}$, we define the IO map $T(G_p, K_p) : (r, -d) \mapsto (e, u)$ in Figure 2 by

$$T(G_p, K_p) = \begin{bmatrix} S_p & S_p G_p \\ K_p S_p & T_p \end{bmatrix}, \quad (9)$$

with $S_p = (1 + G_p K_p)^{-1}$ and $T_p = 1 - S_p$. If $G_p, K_p \in \mathcal{RH}_\infty$, then $T(G_p, K_p)$ is internally stable if all elements in the IO map $T(G_p, K_p)$, defined by (9), are stable. This is implied by $S_p \in \mathcal{RH}_\infty$ [23, Chapter 3]. If $T(G_p, K_p) \in \mathcal{RH}_\infty$ holds for all $p \in \mathbb{P}$, then the closed-loop LPV system is called locally internally stable. Internal stability is important to prevent hidden pole-zero cancellations. To assess internal stability for unstable G_p or K_p , introduce the factorization

$$G_p = N_{G_p} D_{G_p}^{-1}, \quad \{N_{G_p}, D_{G_p}\} \in \mathcal{RH}_\infty. \quad (10)$$

The two transfer functions $\{N_{G_p}, D_{G_p}\}$ are a coprime factorization over \mathcal{RH}_∞ if there exist two other transfer functions $\{X_p, Y_p\} \in \mathcal{RH}_\infty$ such that they satisfy the Bézout identity

$$N_{G_p} X_p + D_{G_p} Y_p = 1. \quad (11)$$

Consequently, $\{X_p Q, Y_p Q\}$ are coprime iff $Q, Q^{-1} \in \mathcal{RH}_\infty$. Correspondingly, K_p admits the coprime factorization

$$K_p = N_{K_p} D_{K_p}^{-1}, \quad \{N_{K_p}, D_{K_p}\} \in \mathcal{RH}_\infty. \quad (12)$$

Using these representations, (9) can be written as

$$T(G_p, K_p) = D_p^{-1} \begin{bmatrix} D_{G_p} D_{K_p} & N_{G_p} D_{K_p} \\ D_{G_p} N_{K_p} & N_{G_p} N_{K_p} \end{bmatrix}, \quad (13)$$

with characteristic equation

$$D_p = D_{G_p} D_{K_p} + N_{G_p} N_{K_p}. \quad (14)$$

The feedback system is internally stable if and only if $D_p^{-1} \in \mathcal{RH}_\infty$. If we set $N_{K_p} = X_p$ and $D_{K_p} = Y_p$, then the characteristic equation (14) equals the Bézout identity (11), thus the feedback system is internally stable as $D_p^{-1} = 1$ and the rest of the terms are stable by design in (13). Similarly, the closed-loop LPV system is called locally internally stable if these conditions hold for all $p \in \mathbb{P}$.

For the transfer $w \mapsto z$, with $w \in \{r, d\}$ and $z \in \{e, u\}$, let

$$T_{z,w}(G_p, K_p) = N_p D_p^{-1}, \quad (15)$$

with $\{N_p, D_p\} \in \mathcal{RH}_\infty$ and $T_{z,w}(G_p, K_p) \in \mathcal{RH}_\infty$, defines the corresponding SISO element of (13). For example, $T_{r,e}(G_p, K_p) = N_p D_p^{-1}$ with $N_p = D_{G_p} D_{K_p}$ defines the sensitivity S_p in (9) and (13).

The following theorem presents analysis conditions to verify internal stability of a closed-loop system locally, given the plant and controller only. As a special case, [20, Theorem 1] is recovered. Here, the idea of coprime factorizations over \mathcal{RH}_∞ is used to allow for unstable plants or controllers, while also extending the result to the class of LPV systems.

Theorem 1. *Let G_p and K_p be as defined in (10) and (12), respectively, and let $D_p \in \mathcal{RH}_\infty$ be as defined in (14). Then the following conditions are equivalent. For all $p \in \mathbb{P}$*

- 1a) $D_p^{-1} \in \mathcal{RH}_\infty$.
 1b) $D_p(s) \neq 0, \forall s \in \mathbb{C}_+ \cup \mathbb{C}_0 \cup \{\infty\}$.
 1c) There exists a multiplier $\alpha_p \in \mathcal{RH}_\infty$ such that
 $\Re\{D_p(i\omega)\alpha_p(i\omega)\} > 0, \forall \omega \in \Omega$.

Proof. For a proof of equivalence between 1a) and 1b), see [23, Chapter 3]. Regarding the equivalence between 1a) and 1c) for all $p \in \mathbb{P}$, note the following reasoning:

(\Rightarrow) Assume 1a) and let $Q = D_p^{-1}$. This implies that the Bézout identity (11) is satisfied for $X_p = N_{K_p}Q$ and $Y_p = D_{K_p}Q$. Hence, 1c) is satisfied by setting $\alpha_p = Q$ because $\Re\{N_{G_p}X_p + D_{G_p}Y_p\} = 1$ for all $\omega \in \Omega$.

(\Leftarrow) Assume 1c) and let $V = D_p\alpha_p$. Note that $V, V^{-1} \in \mathcal{RH}_\infty$ because 1c) implies that $D_p\alpha_p$ is bi-proper and has no right half-plane (RHP) zeros. Then $D_p = V\alpha_p^{-1}$ satisfies the Bézout identity (11), therefore $D_p^{-1} \in \mathcal{RH}_\infty$. Thus 1c) implies 1a) and consequently 1b). This completes the proof. \square

Remark. A direct result of Theorem 1 is that $\alpha_p^{-1} \in \mathcal{RH}_\infty$. This is easy to prove because

- There does not exist a strictly proper $\alpha_p \in \mathcal{RH}_\infty$ such that 1c) holds. Indeed 1c) is violated at $\omega = \infty$.
- There does not exist an $\alpha_p \in \mathcal{RH}_\infty$ with $\alpha_p^{-1} \notin \mathcal{RH}_\infty$ such that 1c) holds. This can be seen as $\alpha_p^{-1} \notin \mathcal{RH}_\infty$ implies that there exists some RHP zero s_0 such that $\alpha_p(s_0) = 0$. Consequently, there exists some frequency ω_0 such that $\Re\{D_p(i\omega_0)\alpha_p(i\omega_0)\} < 0$ and 1c) is violated.

Theorem 1 gives an analysis condition that provides a local stability result for the closed-loop system if instead of a parametric model, N_{G_p} and D_{G_p} are only given in terms of local frequency-domain data. The next subsection presents the extension towards a performance analysis condition.

B. Performance

In this subsection, analysis conditions to assess locally the \mathcal{H}_∞ -performance of an LPV system, given the plant and controller only, are presented. This constitutes contribution C4). To derive performance analysis conditions, the main loop theorem is of importance and is presented first.

Consider the transfer function $T_{z,w}(G_p, K_p) \in \mathcal{RH}_\infty$ of interest in Figure 3a, such that $w \mapsto z : T_{z,w}(G_p, K_p)$, and let $\hat{\Delta} \in \mathbf{B}\hat{\Delta}$, with

$$\mathbf{B}\hat{\Delta} := \left\{ \hat{\Delta} \in \mathcal{RH}_\infty \mid |\hat{\Delta}(i\omega)| < 1, \forall \omega \in \Omega \right\} \quad (16)$$

a fictitious uncertainty, represent the \mathcal{H}_∞ -performance criterion. Then, the \mathcal{H}_∞ -performance of the system in Figure 3a is equivalent to Figure 3b [24, Theorem 8.7]. This is stated in terms of the following theorem, where the weighting filter W_T is introduced to specify the frequency-dependent design requirements on the map $w \mapsto z$.

Theorem 2 (Main loop theorem). Let $W_T \in \mathcal{RH}_\infty$ and $T_{z,w}(G_p, K_p)$ be defined as in (15). The following statements are equivalent. For all $p \in \mathbb{P}$

- $\sup_{\omega \in \Omega} |W_T(i\omega)T_{z,w}(G_p, K_p)(i\omega)| \leq \gamma$.
- $1 - \gamma^{-1}W_T(i\omega)T_{z,w}(G_p, K_p)(i\omega)\hat{\Delta}(i\omega) \neq 0,$
 $\forall \omega \in \Omega, \forall \hat{\Delta} \in \mathbf{B}\hat{\Delta}$.

Theorem 2 is a special case of [25, Theorem 11.7].

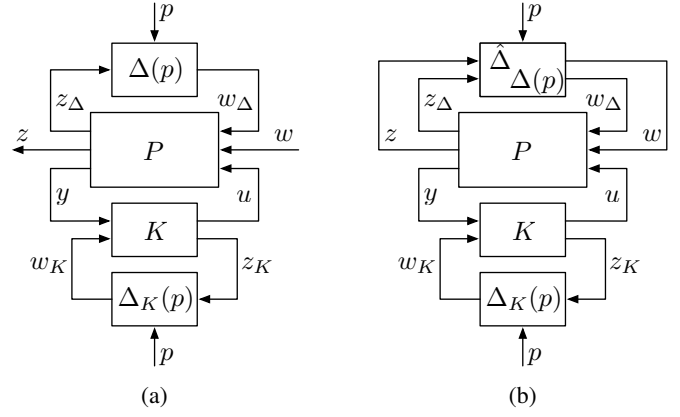


Fig. 3: Generalized LPV plant (a); and performance of the SISO closed-loop map $w \mapsto z$ (b).

Remark. By Theorem 2, nominal performance can be seen as a special case of robust stability, where a fictitious uncertainty is connected to the performance channel, see Figure 3b.

In the data-driven setting, the absence of a parametric model of $T_{z,w}(G_p, K_p)$ makes it difficult to turn 2b) into a convex constraint as it is generally done in LPV synthesis approaches for gain-scheduling [6]. Hence, in that case 2b) is needed to be evaluated for an infinite set of realizations of the fictitious uncertainty $\hat{\Delta}$, for example, as in [26]. The contribution in this paper is to utilize Theorem 1 together with Theorem 2 to derive a single condition to analyze both stability and performance without the need to sample $\hat{\Delta}$.

Theorem 3. Let $W_T \in \mathcal{RH}_\infty$ and $T_{z,w}(G_p, K_p)$ be defined as in (15). Requirements R1) and R2) are satisfied if and only if there exists a multiplier $\alpha_p \in \mathcal{RH}_\infty$ such that

$$\Re\{(D_p(i\omega) - \gamma^{-1}|W_T(i\omega)N_p(i\omega)|)\alpha_p(i\omega)\} > 0, \quad (17)$$

$$\forall \omega \in \Omega, \forall p \in \mathbb{P}.$$

Proof. Requirement R2) can be equivalently stated using Theorem 2, Condition 2b), i.e.,

$$1 - \gamma^{-1}W_T(i\omega)T_{z,w}(G_p, K_p)(i\omega)\hat{\Delta}(i\omega) \neq 0, \quad (18)$$

$$\forall \omega \in \Omega, \forall p \in \mathbb{P}, \forall \hat{\Delta} \in \mathbf{B}\hat{\Delta}.$$

As $D_p \in \mathcal{RH}_\infty$, $D_p(i\omega) \neq 0, \forall \omega \in \Omega$ and by multiplying (18) with it, the resulting non-singularity condition is:

$$D_p(i\omega) - \gamma^{-1}W_T(i\omega)N_p(i\omega)\hat{\Delta}(i\omega) \neq 0, \quad (19)$$

$$\forall \omega \in \Omega, \forall p \in \mathbb{P}, \forall \hat{\Delta} \in \mathbf{B}\hat{\Delta}.$$

Based on a homotopy argument, (19) corresponds to Condition 1b) in Theorem 1, which through 1c) is equivalent with

$$\Re\{(D_p(i\omega) - \gamma^{-1}W_T(i\omega)N_p(i\omega)\hat{\Delta}(i\omega))\alpha_p(i\omega)\} > 0, \quad (20)$$

$$\forall \omega \in \Omega, \forall p \in \mathbb{P}, \hat{\Delta} \in \mathbf{B}\hat{\Delta}.$$

When $\hat{\Delta} = 0 \in \mathbf{B}\hat{\Delta}$, (20) reduces to $\Re\{D_p(i\omega)\alpha_p(i\omega)\} > 0$, which is the same as Condition 1c) in Theorem 1, hence (20) implies requirement R1).

Let $1 \geq \epsilon > 0$ and consider (20) on

$$\mathbf{B}_\epsilon \hat{\Delta} := \left\{ \hat{\Delta} \in \mathcal{RH}_\infty \mid |\hat{\Delta}(i\omega)| \leq 1 - \epsilon, \forall \omega \in \Omega \right\}, \quad (21)$$

which is the scaled closed uncertainty ball contained in $\mathbf{B}\hat{\Delta}$. Since any $\hat{\Delta} \in \mathbf{B}_\epsilon \hat{\Delta}$ represents a rotation and contraction

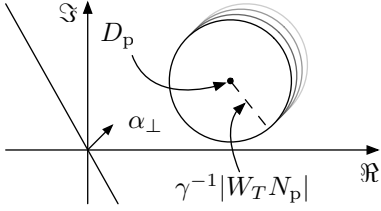


Fig. 4: Illustration of stability and \mathcal{H}_∞ -performance. The transfer function α_p represents, for each frequency, a line passing through the origin. If this line does not intersect with the disks $D_p - \gamma^{-1}|W_T N_p|$, then the disks exclude the origin and (18) must hold.

in the complex plane, it is necessary and sufficient to check (20) on the boundary only, i.e., for $\hat{\Delta} \in \partial \mathbf{B}_\epsilon \hat{\Delta}$, with $|\hat{\Delta}(i\omega)| = 1 - \epsilon$, $\forall \omega \in \Omega$. Note that, in (20), $W_T(i\omega)N_p(i\omega)$ only represents complex scaling of this ball which is centered at $D_p(i\omega)$. Hence, (20) restricted on $\mathbf{B}_\epsilon \hat{\Delta}$ is equivalent with

$$\Re\{(D_p(i\omega) - \gamma^{-1}(1 - \epsilon)|W_T(i\omega)N_p(i\omega)|)\alpha_p(i\omega)\} > 0, \quad \forall \omega \in \Omega, \forall p \in \mathbb{P}. \quad (22)$$

This means that if (22) holds, then violation of (20) can only happen in $\mathbf{B}_\epsilon \hat{\Delta} \setminus \mathbf{B}_\epsilon \hat{\Delta}$. As (22) is continuous in ϵ , by taking the limit $\epsilon \rightarrow 0$, $\mathbf{B}_\epsilon \hat{\Delta} \setminus \mathbf{B}_\epsilon \hat{\Delta} \rightarrow \emptyset$ and we obtain that (17) is equivalent with (20). \square

Theorem 3 states that the performance condition 2a) is satisfied if and only if for each frequency $\omega \in \Omega$ and scheduling value $p \in \mathbb{P}$ the disks with radius $\gamma^{-1}|W_T N_p|$, centered at D_p , do not include the origin. This holds if there exists $\alpha_p \in \mathcal{RH}_\infty$, representing for each frequency a line passing through the origin, that does not intersect with the disks, see Figure 4. The analysis condition is especially useful as it provides a local stability and performance result given a controller and the data $\mathcal{D}_{N,p,\tau}$.

If the fFRFs are subject to model uncertainty, robust stability and performance have to be taken into account [15].

C. Synthesis

It turns out that it is possible to give an equivalent formulation of Theorem 3 which enables controller synthesis.

Theorem 4. *Given $G_p = N_{G_p} D_{G_p}^{-1}$, with $\{N_{G_p}, D_{G_p}\} \in \mathcal{RH}_\infty$ coprime, as defined in (10), and a weighting filter $W_T \in \mathcal{RH}_\infty$, the following statements are equivalent.*

4a) *There exists a proper rational controller K_p that achieves internal stability and performance as defined in requirements R1) and R2), respectively.*

4b) *There exists a controller $K_p = N_{K_p} D_{K_p}^{-1}$, with $\{N_{K_p}, D_{K_p}\} \in \mathcal{RH}_\infty$, as defined in (12), such that*

$$\Re\{D_p(i\omega)\} > \gamma^{-1}|W_T(i\omega)N_p(i\omega)|, \quad \forall \omega \in \Omega, \forall p \in \mathbb{P}. \quad (23)$$

Proof. (\Rightarrow) Assume $K_p = \tilde{N}_{K_p} \tilde{D}_{K_p}^{-1}$ satisfies 4a). Then, by Theorem 3, there exists an $\alpha_p \in \mathcal{RH}_\infty$ such that (17) holds. Choosing $N_{K_p} = \tilde{N}_{K_p} \alpha_p$, $D_{K_p} = \tilde{D}_{K_p} \alpha_p$ results in $K_p = N_{K_p} D_{K_p}^{-1} = \tilde{N}_{K_p} \tilde{D}_{K_p}^{-1}$ and consequently 4b) holds.

(\Leftarrow) Assume 4b) holds. Because $D_p \in \mathcal{RH}_\infty$ and $D_p(i\omega)$ is positive for all $\omega \in \Omega$, $\{N_{K_p}, D_{K_p}\}$ form Bézout factors for $\{N_{G_p}, D_{G_p}\}$. Thus by Theorem 1, $D_p^{-1} \in \mathcal{RH}_\infty$ and

K_p internally stabilizes G_p and R1) holds. By Theorem 3, requirement R2) holds. This completes the proof. \square

Theorem 4 presents a local \mathcal{H}_∞ -optimal controller synthesis condition given only data $\mathcal{D}_{N,p,\tau}$. This is further developed in Section IV, where an optimization problem is formulated and the controller parameterization is discussed.

Remark. *Theorem 4 shows that the multiplier α_p can be absorbed into the controller as $\gamma^{-1}|W_T(i\omega)N_p(i\omega)\alpha_p(i\omega)| \Rightarrow \Re\{\gamma^{-1}|W_T(i\omega)N_p(i\omega)|\alpha_p(i\omega)\}$. Note that the absorbed multiplier changes the considered N_p and D_p , but α_p cancels out when $K_p = N_{K_p} D_{K_p}^{-1}$ is computed. The price to be paid for this absorption is the increased order of N_{K_p} and D_{K_p} .*

Remark. [15, Theorem 1] is recovered in the special case when the plant and controller are LTI.

IV. CONTROLLER SYNTHESIS

In this section, we build upon the stability and performance analysis and synthesis conditions derived in Section III by developing a procedure to synthesize LPV controllers. This forms Contribution C1). First, an optimization problem is set up in Section IV-A that characterizes the synthesis problem based on Theorem 4. This is followed by a discussion on the controller parameterization in Section IV-B and implementation aspects in Section IV-C.

A. Controller synthesis

Given the data $\mathcal{D}_{N,p,\tau}$ and a controller parameterization $K_p = N_{K_p} D_{K_p}^{-1}$, given in the Section IV-B, an optimization problem is formulated satisfying requirements R1) and R2).

$$\begin{aligned} \min_{\theta, \gamma} \quad & \gamma \\ \text{s.t.} \quad & \gamma \Re\{D_p(i\omega, \theta)\} > |W_T(i\omega)N_p(i\omega, \theta)| \\ & \forall \omega \in \Omega, p \in \mathcal{P} \end{aligned} \quad (24)$$

where θ are the controller parameters.

The optimization problem (24) is in general non-convex. However, through a linear parameterization of the controller, (24) becomes a quasi-convex optimization problem in the controller parameters θ and the performance indicator γ . To solve the quasi-convex program, a bisection algorithm over γ is utilized. This results in an iterative approach, where for every fixed value of γ , a second-order cone program is solved.

To provide stability and performance guarantees, the constraints in (24) need to be satisfied for all $\omega \in \Omega$, which is an infinite set, leading to a semi-infinite program. One solution is to solve (24) for a finite set of frequencies $\Omega_N = \{\omega_k\}_{k=1}^N \subset \Omega$. The frequency set can be chosen randomly, according to the scenario approach [27]. This allows for the computation of confidence bounds on the constraints. In the data-driven setting this choice is spared from the user as the data is only available at a pre-specified set of frequency points. Either of these methods result in a quasi-convex second-order cone program and can be solved as described above.

B. Controller parameterization

An orthonormal basis function (OBF)-based representation [21] is a natural choice to parameterize the controller factors

$$N_{K_p}(s) = \sum_{i=0}^{n_N} w_i(p) \phi_i(s), \quad (25a)$$

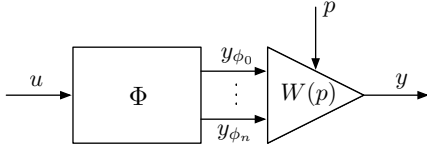


Fig. 5: Input-output graph of the Wiener LPV OBF structure.

$$D_{K_p}(s) = \sum_{i=0}^{n_D} v_i(p) \varphi_i(s), \quad (25b)$$

Here, $\{\phi_i\}_{i=0}^{n_N}$ and $\{\varphi_i\}_{i=0}^{n_D}$ with $\phi_0 = \varphi_0 = 1$ and $n_D \geq n_N$ are the sequence of basis functions, with coefficient functions

$$w_i(p) = \sum_{\ell=1}^m \check{w}_i^\ell \psi_\ell(p), \quad v_i(p) = \sum_{\ell=1}^m \check{v}_i^\ell \psi_\ell(p). \quad (26)$$

Here, the coefficient functions are formed through a chosen functional dependence, e.g., affine, polynomial or rational, characterized by the basis functions $\{\psi_\ell\}_{\ell=1}^m$. See [21, Chapter 9.2] for an overview of OBF based LPV model structures. The OBF controller parameterization enables tuning of both the poles and zeros of the controller, in contrast to previous data-driven frequency-domain LPV tuning methods [17]–[19]. Additional controller requirements are discussed in [28].

Local aspects of (25a)–(25b) can be preserved by considering a time-domain Wiener LPV OBF realization

$$y_{N_{K_p}}(t) = \sum_{i=0}^{n_N} w_i(p(t)) y_\phi(t), \quad (27a)$$

$$y_{D_{K_p}}(t) = \sum_{i=0}^{n_D} v_i(p(t)) y_\phi(t), \quad (27b)$$

with $y_\phi = \Phi u$. The parameterization of N_{K_p} and D_{K_p} can be viewed as a bank of OBFs, whose output is weighted with parameter-dependent coefficient functions, see Figure 5.

Equations (27a)–(27b) reveal that requirements (i)–(iv) are satisfied. Requirement (v) is satisfied, w.l.o.g. by $\{\check{v}_i^\ell\}_{i=0}^\ell = \{1, 0, \dots, 0\}$. Because the set of bases is complete w.r.t. \mathcal{H}_2 , hence any solution including the optimal solution of (24) can be found via parameterizations (25a)–(25b) [15].

Remark. Note that (27a) and (27b) depend on time-varying p and characterize the global behavior of the factors N_{K_p} and D_{K_p} . The concept in this paper is to tune the parameter-dependent coefficient functions based on their local behavior, i.e., (25a)–(25b) for constant p , in-line with the data $\mathcal{D}_{N,p\tau}$.

Algorithm 1 presents the selection of optimal OBFs, based on the Kolmogorov n -Width theory. Given a desired number of poles, an optimal set of OBFs is selected based on Fuzzy Kolmogorov c -Max (FKcM) clustering of the poles, such that the decay rate of the OBFs is minimized [21, Chapter 8].

Algorithm 1: Basis function selection

- 1 Choose arbitrary bases $\{\phi_i\}_{i=0}^{n_N}$ and $\{\varphi_i\}_{i=0}^{n_D}$, solve (24) for $\theta = \{\{\check{w}_i^\ell\}_{\ell=1}^m \cup \{\check{v}_i^\ell\}_{\ell=1}^m\}$ and compute \hat{N}_{K_p} and \hat{D}_{K_p} .
 - 2 Given \hat{N}_{K_p} and \hat{D}_{K_p} , compute the corresponding local pole and zero variations of the controller. Choose new bases $\{\phi_i\}$ and $\{\varphi_i\}$ based on FKcM clustering of the poles and zeros.
 - 3 Solve (24) and compute N_{K_p} and D_{K_p} .
 - 4 Stop if a desired performance and order of the bases has been achieved, otherwise go to step 2.
-

C. Controller implementation

The OBF parameterizations admit a linear fractional representation (LFR). In this representation, the dependency on

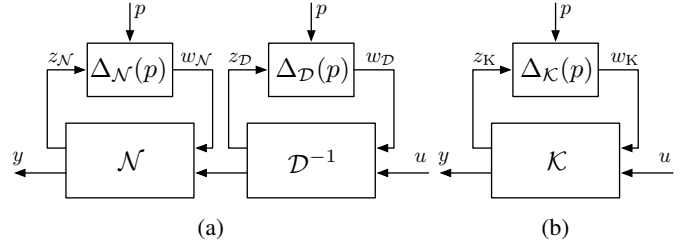


Fig. 6: Controller realization through (a) the series connection of the LFRs $N_{K_p} = \mathcal{F}_u(\mathcal{N}, \Delta_{\mathcal{N}}(p))$ and $D_{K_p} = \mathcal{F}_u(\mathcal{D}^{-1}, \Delta_{\mathcal{D}}(p))$ and (b) $K_p = \mathcal{F}_u(\mathcal{K}, \Delta_{\mathcal{K}})$, with $\Delta_{\mathcal{K}} = \text{diag}(\Delta_{\mathcal{N}}, \Delta_{\mathcal{D}})$.

the scheduling variable p is extracted by formulating (27a) and (27b) in terms of LTI systems, denoted \mathcal{N} and \mathcal{D} , such that $N_{K_p} = \mathcal{F}_u(\mathcal{N}, \Delta_{\mathcal{N}}(p))$ and $D_{K_p}^{-1} = \mathcal{F}_u(\mathcal{D}^{-1}, \Delta_{\mathcal{D}}(p))$, respectively, where \mathcal{F}_u is the upper linear fractional transformation [25], see Figure 6a. The inverse \mathcal{D}^{-1} is obtained through partial inversion of the IO map, see, e.g., [25, Chapter 10]. The controller is formed through the series connection of the LFRs \mathcal{N} and \mathcal{D}^{-1} , resulting in the LFR \mathcal{K} such that $K_p = \mathcal{F}_u(\mathcal{K}, \text{diag}(\Delta_{\mathcal{N}}, \Delta_{\mathcal{D}}))$, see Figure 6b.

V. CONTROL DESIGN FOR THE CMG

In this section, a controller is designed and implemented on the CMG. Although the theory in this paper is presented in continuous-time, with this example we show that a discrete-time application is possible. The system identification and controller design are performed at a sampling rate of 200 Hz.

A. Frequency-domain measurements

As described in Section II, the dynamics of the CMG are dependent on the velocity of the disk. It is therefore natural to consider the velocity $\dot{q}_1(t) = p(t)$ as a scheduling variable. The disk velocity operates in the range $\mathbb{P} = [30, 50]$ rad/s. To identify the local behavior at different disk velocities, an equidistant grid $\mathcal{P} = \{30, 40, 50\}$ is chosen. As the gyroscope is inherently an unstable system, the measurements are performed in closed-loop using a stabilizing LTI controller.

The coprime factors $N_{G_p}(i\omega)$ and $D_{G_p}(i\omega)$ can be calculated from the estimates of the process sensitivity $S_p G_p$ and sensitivity S_p , respectively [15]. This is achieved by estimating the fFRF of the mappings $d \mapsto y$ and $d \mapsto u_G$, respectively, in Figure 2. During a closed-loop experiment, the system is excited by a white-noise disturbance signal d . The position of gimbal A is measured with an optical encoder. Data records with a length of 240000 samples are collected for each operating point $p \in \mathcal{P}$.

The obtained fFRFs are estimated using the empirical transfer function estimate, using a Hanning window, and contain 1000 frequency points per operating point. Figure 7 shows the estimated fFRFs G_p . The figure highlights that the system is subject to a relatively high noise level, which has a significant effect at higher frequencies. The scheduling dependency is also clear to see, which manifests in terms of a shift in the resonance frequencies and the low-frequency gain.

B. Data-driven controller synthesis

The goal is to control the position q_4 of gimbal A by actuating gimbal C through torque τ_2 . To highlight the parameter dependence, the objective is to track a reference signal subject

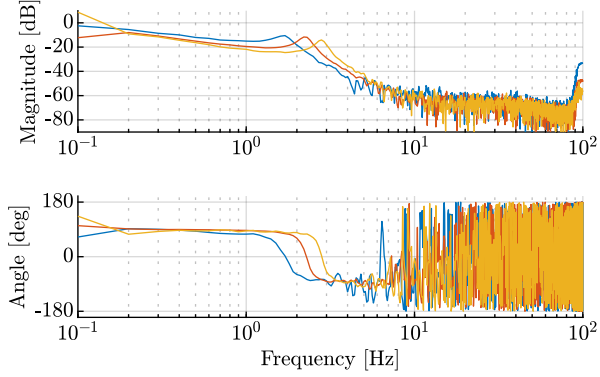


Fig. 7: Bode plot of the estimated fFRFs of G_p for the three grid points $p \in \mathcal{P} = \{30, 40, 50\}$ in blue, orange and yellow, respectively. A parameter-varying shift in resonance frequencies and low-frequency gain is observed.

to variations in the disk velocity. To specify this objective in terms of control design, consider the full 4-block shaping problem in Figure 2. Based on the fFRFs in Figure 7, the first resonance occurs at 1.7 Hz. The shaping filters are designed such that a bandwidth of 0.75 Hz is achieved. The sensitivity is shaped to provide a lower bound on the bandwidth and to limit the overshoot by providing an upper bound of 6 dB for higher frequencies. Integral action is desired to achieve 0 steady-state error. To suppress the effects of measurement noise while also limiting high-frequency control actions, a high-frequency roll-off is enforced into the controller by shaping the control and complementary sensitivities. Shaping the complementary sensitivity also provides an upper bound on the achieved bandwidth. The process sensitivity is restricted to lie below 0 dB to limit the amplification of disturbances.

Using the approach presented in this paper, an LPV and LTI controller are synthesized, for which the results are given in Figures 8 and 9. Both controllers are parameterized by discrete-time Laguerre bases of orders $n_K = n_D = 5$ with pole $z = 0.7$. The LPV controller has affine scheduling-dependence, and the LTI controller is scheduling-independent. The achieved performance levels are $\gamma_{\text{LPV}} = 1.2097$ and $\gamma_{\text{LTI}} = 3.1792$. The LTI controller does not meet the performance criteria for all operating points and, therefore has to sacrifice performance in order to achieve robust performance. The LPV controller achieves good performance for the considered operating space by compensating for the parameter-dependent low-frequency gain and resonance behavior.

C. Results

First, the tracking performance is evaluated locally, when the scheduling variable operates at constant velocities $\mathcal{P} = \{30, 40, 50\}$ rad/s. Figure 10 shows the measured step responses using the designed LPV and LTI controllers. The main differences are observed for $p = 30$ and $p = 50$ rad/s. At $p = 30$ rad/s, the step response shows a significant oscillation when using the LTI controller. This oscillation corresponds to the resonance frequency at 1.7 Hz in Figure 8 and it is significantly larger compared to the LPV case. For $p = 50$ rad/s, a slightly higher bandwidth is achieved when using the LPV controller, which corresponds to a faster rise and settling

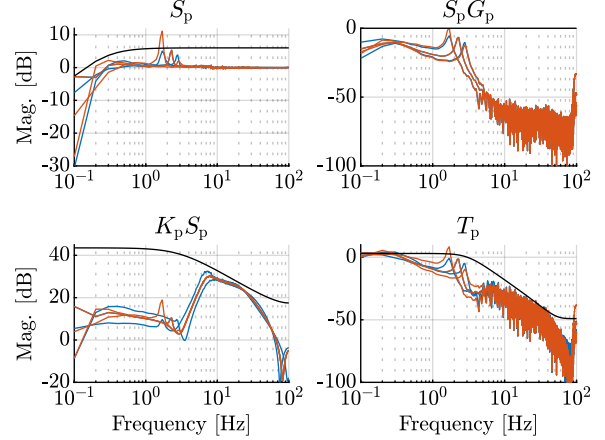


Fig. 8: Magnitude plots of the fFRFs of the 4-block (9). The LPV and LTI designs are shown in blue and orange, respectively. The weighting filters are shown in black. The LTI controller design does not meet the performance specifications.

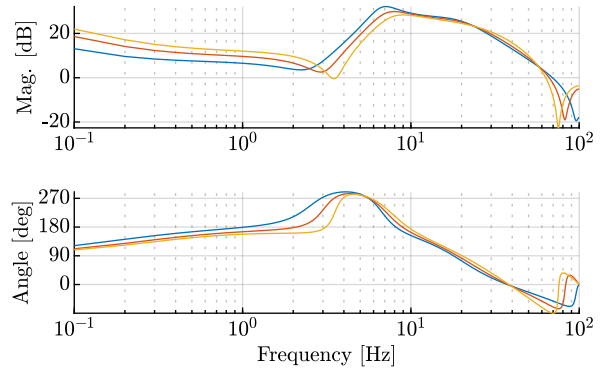


Fig. 9: Magnitude and phase plots of the LPV controller for frozen scheduling-values $\mathcal{P} = \{30, 40, 50\}$ in blue orange and yellow, respectively. The LPV controller compensates the parameter-varying low-frequency gain and resonance behavior observed in Figure 7.

time. Finally, the responses when using the LPV controller are very consistent, with only a small variation in settling time.

Next, the performance is evaluated for a time-varying scheduling variable. A Square wave reference signals, filtered with a 3rd order low-pass filter with a cut-off frequency of 0.7 Hz, are used to challenge the system. The amplitude of the reference is 15° . The scheduling variable, i.e. the disk velocity, tracks a similar, but faster square wave trajectory in the range $\mathbb{P} = [30, 50]$ rad/s. Implementation of the controller is done according to the LFR representation described in Section IV-C, where the controller is scheduled at each sampling interval.

Figure 11 shows the reference signal, tracking performance, scheduling variation and control effort for the designed LPV and LTI controllers. The results indicate that the LPV controller performs significantly better than the LTI controller. A reduction in overshoot and settling time are observed. More specifically, we obtain a 39% and 33% decrease between the ℓ_2 and ℓ_∞ norms of the error signals, respectively. These results experimentally validate the capabilities of the proposed control methodology, including the benefit of using an LPV controller over an LTI controller for the CMG. However, it is imperative to note that stability and performance guarantees are provided only locally. Hence, stability and performance of the nonlinear

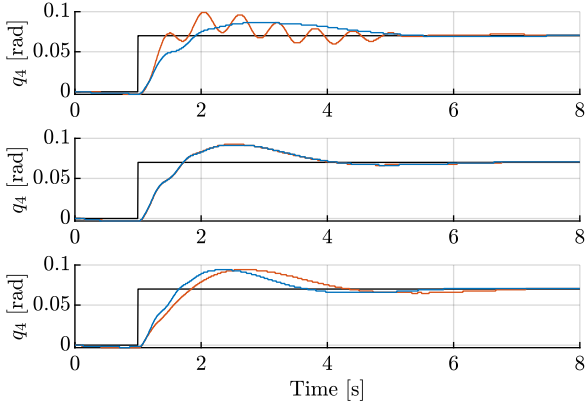


Fig. 10: Measured local step responses of the CMG for constant scheduling variables $\mathcal{P} = \{30, 40, 50\}$ rad/s, from top to bottom, respectively. The angle of gimbal A is shown in blue and orange when using the LPV and LTI controller, respectively. The LTI design loses performance for $p \in \{30, 50\}$ rad/s, whereas the LPV design displays consistent results for the considered operating points.

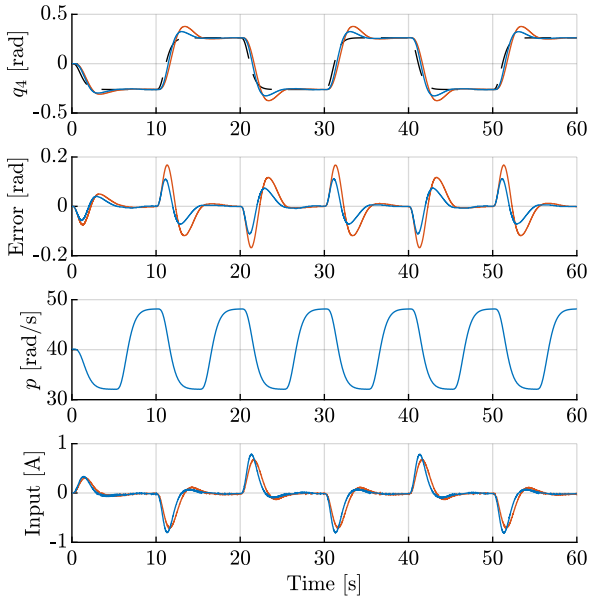


Fig. 11: Experimental results of the CMG. The top figure shows the reference (black) and the angle of gimbal A when using the LPV and LTI controllers in blue and orange, respectively. The other figures shows the error, scheduling and input signals. The LPV design significantly improves the performance by decreasing the overshoot.

system can only be guaranteed for sufficiently slow variations of the scheduling variable.

VI. CONCLUSION

The LPV controller synthesis approach in this paper enables the design of operating condition-dependent controllers directly from frequency-domain data. Experimental demonstrations on a control moment gyroscope show that significant increase in performance can be achieved via the proposed approach for operating condition-dependent systems. In comparison to existing methods in the literature, this approach enables the design of rational LPV controllers, for which local stability and performance analysis certificates are provided.

Future research aims at global stability and performance guarantees.

REFERENCES

- [1] R. Kristiansen, O. Egeland, and P. J. Nicklasson, "A comparative study of actuator configurations for satellite attitude control," *Modeling, Identification and Control*, 2005.
- [2] B. Wie, *Space vehicle dynamics and control*. American Institute of Aeronautics and Astronautics, 2008.
- [3] R. Tóth, M. van de Wal, P. S. Heuberger, and P. M. Van den Hof, "LPV identification of high performance positioning devices," in *Proc. of the Am. Control Conf.*, 2011.
- [4] H. S. Abbas, A. Ali, S. M. Hashemi, and H. Werner, "LPV state-feedback control of a control moment gyroscope," *Control Engineering Practice*, 2014.
- [5] V. Preda, "Robust microvibration control and worst-case analysis for high pointing stability space missions," Ph.D. dissertation, 2017.
- [6] C. Hoffmann and H. Werner, "A survey of linear parameter-varying control applications validated by experiments or high-fidelity simulations," *IEEE Trans. Control Syst. Technol.*, 2015.
- [7] T. Oomen, "Advanced motion control for precision mechatronics: Control, identification, and learning of complex systems," *IEEJ Journal of Industry Applications*, 2018.
- [8] R. Pintelon and J. Schoukens, *System Identification: A Frequency Domain Approach*, 2nd ed. John Wiley & Sons, 2012.
- [9] R. van der Maas, A. van der Maas, R. Voorhoeve, and T. Oomen, "Accurate FRF identification of LPV systems: nD-LPM with application to a medical X-ray system," *IEEE Trans. Control Syst. Technol.*, 2017.
- [10] J. M. Maciejowski, "Multivariable feedback design," *Addison-Wesley*, 1989.
- [11] H. Hjalmarsson, "From experiment design to closed-loop control," *Automatica*, 2005.
- [12] E. Grassi, K. S. Tsakalis, S. Dash, S. V. Gaikwad, W. MacArthur, and G. Stein, "Integrated system identification and PID controller tuning by frequency loop-shaping," *IEEE Trans. Control Syst. Technol.*, 2001.
- [13] S. Khadraoui, H. Nounou, M. Nounou, A. Datta, and S. P. Bhat-tacharyya, "A model-free design of reduced-order controllers and application to a DC servomotor," *Automatica*, 2014.
- [14] A. Karimi, M. Kunze, and R. Longchamp, "Robust controller design by linear programming with application to a double-axis positioning system," *Control Engineering Practice*, 2007.
- [15] A. Karimi, A. Nicoletti, and Y. Zhu, "Robust \mathcal{H}_∞ controller design using frequency-domain data via convex optimization," *Int. J. Robust Nonlin Control*, 2018.
- [16] S. Formentin, D. Piga, R. Tóth, and S. M. Savaresi, "Direct learning of LPV controllers from data," *Automatica*, 2016.
- [17] M. Kunze, A. Karimi, and R. Longchamp, "Gain-scheduled controller design by linear programming," in *Proc. of the Eur. Control Conf.*, 2007.
- [18] A. Karimi and Z. Emedi, " \mathcal{H}_∞ gain-scheduled controller design for rejection of time-varying narrow-band disturbances applied to a benchmark problem," *European Journal of Control*, 2013.
- [19] T. Bloemers, R. Tóth, and T. Oomen, "Towards Data-Driven LPV Controller Synthesis Based on Frequency Response Functions," in *Proc. of the IEEE Conf. Decis. Control*, 2019.
- [20] A. Rantzer and A. Megretski, "A Convex Parameterization of Robustly Stabilizing Controllers," *IEEE Trans. Autom. Control*, 1994.
- [21] R. Tóth, *Modeling and identification of linear parameter-varying systems*. Springer, Heidelberg, 2010.
- [22] M. Schoukens and R. Tóth, "Frequency response functions of linear parameter-varying systems," in *Proc. of the 3rd IFAC Workshop on Linear Parameter-Varying Systems*, 2019.
- [23] J. C. Doyle, B. A. Francis, and A. R. Tannenbaum, *Feedback Control Theory*. Macmillan Publishing Co., 1992.
- [24] S. Skogestad and I. Postlethwaite, *Multivariable Feedback Control Analysis and design*, 2nd ed. John Wiley & Sons, 2001.
- [25] K. Zhou, J. C. Doyle, K. Glover *et al.*, *Robust and optimal control*. Prentice hall, New Jersey, 1996.
- [26] E. van Solingen, J. van Wingerden, and T. Oomen, "Frequency-domain optimization of fixed-structure controllers," *Int. J. Robust Nonlin Control*, 2018.
- [27] G. C. Calafiore and M. C. Campi, "The scenario approach to robust control design," *IEEE Trans. Autom. Control*, 2006.
- [28] T. Bloemers, R. Tóth, and T. Oomen, "Frequency-domain data-driven controller synthesis for unstable LPV systems," in *Proc. of the 4th IFAC Workshop on Linear Parameter-Varying Systems*, 2021.